Journal of
Applied
Crystallography

ISSN 0021-8898

Received 17 October 2012
Accepted 8 July 2013

Innovative insights in a plug flow microreactor for *operando* X-ray studies

Santiago J. A. Figueroa,[a]*‡ Dean Gibson,[a] Trevor Mairs,[a] Sebastien Pasternak,[a] Mark A. Newton,[a] Marco Di Michiel,[a] Jerome Andrieux,[a]¶ Konstantinos C. Christoforidis,[b] Ana Iglesias-Juez,[b] Marcos Fernández-García[b] and Carmelo Prestipino[c]

[a]European Synchrotron Radiation Facility, Jules Horowitz 6/BP220, Grenoble, 38043, France, [b]Instituto de Catálisis y Petroleoquímica, CSIC, Marie Curie 2, Cantoblanco, Madrid, 28049, Spain, and [c]Institute Sciences Chimiques de Rennes UMR 6226, CNRS, Campus de Beaulieu, Rennes, 35042, France. Correspondence e-mail: santiago.figueroa@lnls.br

Different solutions have been proposed over the years to optimize control of the temperature and atmosphere over a catalyst in order to reach an ideal reactor behavior. Here, a new innovative solution which aims to minimize temperature gradients along the catalyst bed is demonstrated. This was attained by focusing the infrared radiation generated from the heating elements onto the catalyst bed with the aid of an aluminium shield. This method yields a $\sim$0.13 K mm^{-1} axial temperature gradient ranging from 960 to 1173 K. With the selection of appropriate capillaries, pressures of 20 bar (2 MPa) can be attained.

1. Introduction

There is an increasing importance linked to the application of *operando* techniques to study heterogeneous catalysis for the exploration of often complex structure–property relationships. It should be noted that only by measuring the reactant conversion or the product formation rate is one able to be certain that the catalysts are behaving and performing as expected. Moreover, as the surface as well as occasionally the bulk structure of catalysts can be modified under reaction conditions, the use of techniques such as spectroscopy or diffraction are required, enabling the investigation of catalysts under actual conditions of operation. This type of characterization enhances our overall understanding of the catalytic process, allowing a direct correlation between the catalyst properties and the activity and/or selectivity to be established and thus providing clues that help to determine the active reaction sites/phases within the catalyst.

The core of an *operando* X-ray study is the reaction cell used to house the catalyst in the X-ray beam, making it possible to specify and control the reactant flow of gasses to the catalyst being studied. Since Clausen *et al.* (1991) introduced the first X-ray diffraction (XRD)-adapted plug flow reactor, many variants on this overall theme have been produced (Li *et al.*, 2001; Grunwaldt *et al.*, 2004; Bare *et al.*, 2007; Chupas *et al.*, 2008; van Beek *et al.*, 2011). However, as Meunier and others have already demonstrated, spectroscopic cells are not usually ideal catalytic reactors (Meunier, 2010) for several reasons. These reasons include temperature gradients (axial and radial) along the catalyst bed and components that may by themselves be unstable or reactive under reaction conditions. To avoid the latter of these problems, the reactor itself must not contain any element that can be catalytically active, thus making the reactor catalytically inert. To address the issue of isothermality and temperature gradients, we propose an innovative idea that has come about by working on the plug flow microreactor model proposed by Chupas *et al.* (2008). This initial design was rebuilt, primarily to make dispersive extended X-ray absorption fine-structure spectroscopy (EXAFS) studies more tenable but also to improve overall usability aspects.

To reduce the presence of any thermal gradients, a circular aluminium shield has been implemented within the heating system and around the capillary itself. Aluminium acts to reflect IR light extremely well. By combining this property with an appropriate geometry that focuses the radiation onto the catalyst bed, this configuration is able to minimize axial temperature gradients along the bed at high temperatures, reaching values of $\sim$0.13 K mm^{-1} under working conditions. The aluminium shield has appropriately determined cutouts for the incoming and transmitted X-rays, which are optimized for performing experiments in transmission and fluorescence geometries. The incorporation of the shield does not compromise the performance of the reactor for total scattering studies, which were the original purpose of the design.

The background scattering contribution derived from the shield is negligible and easily removed, making this design usable for experiments that are sensitive to parasitic X-ray scattering.

The addition of a second capillary in the cell was originally a result of considering applications involving dispersive EXAFS, wherein a suitable reference is required to obtain EXAFS measurements from certain types of material (Newton, 2007). However, the addition of this second capillary has also been useful for other reasons, such as allowing measurements of references or two simultaneous thermal treatments during variable-temperature data collections, thereby increasing the overall efficiency of experimentation time. The catalytic properties together with activity, selectivity and stability can be evaluated during the structural and electronic characterization by using a mass spectrometer or a micro gas chromatograph installed in

‡ Present address: Centro Nacional de Pesquisa em Energia e Materiais (CNPEM), Laboratório Nacional de Luz Síncrotron (LNLS), Rua Giuseppe Maximo Scolfaro, 10.000, Polo II de Alta Tecnologia, Caixa Postal 6192, 13083-970 Campinas, SP, Brazil.
¶ Present address: Universite Claude Bernard Lyon 1, 43 Boulevard du 11 Novembre 1918, 69622 Villeurbanne-Cedex, Lyon, France.

the microreactor outlet. According to our laboratory tests, we are able to perform flow pressure measurements of up to 20 bar (1 bar = 10^5 Pa). Consequently, this cell allows us to conduct *operando* experiments on working powder catalysts under industrially relevant conditions (Bare *et al.*, 2011).

2. Cell description and performance

As illustrated in Fig. 1, the reactor is built using modular components that are sufficiently robust to give the necessary assembly flexibility. The oven itself is mounted in a 50 mm-square aluminium profile which contains two support-welded Swagelok fittings (1/8″ Swagelok). One of these supports is permanently fixed, which corresponds to the exhaust part of the reactor. The support consists of a T-piece holding a thermocouple that can be placed inside the capillary close to the sample, as shown in Fig. 1. In order to optimize flow, decrease dead volumes and make the radial gradients along the bed negligible, we have attempted to minimize all the possible flow dimensions (Meunier, 2010). For this reason, we use up to 1.6 mm-external-diameter quartz capillaries. The wall thickness is selected depending on the X-ray energy used as well as the pressure range required for the measurement. The usual thickness ranges from 0.01 mm up to 0.2 mm. The combination of thin capillary walls with small sample volumes is crucial to achieve a good heat transmission and allow a finely controllable heating environment (Jacques *et al.*, 2009).

For low-temperature operation (maximum 673 K), the use of Kapton capillaries is viable. The catalyst powder is first adequately sieved (Jacques *et al.*, 2009) and placed in between two quartz wool plugs to prevent blow out during operation. At this stage the capillary is slid into the thermocouple as close to the bed as possible (1 mm or less) and glued into the stainless steel tubes with a high-temperature epoxy glue (van Beek *et al.*, 2011). This solution prevents air leaks and avoids any unnecessary mechanical tension on the capillaries derived from the use of ferrules, which are the main source of capillary failure in such arrangements. The movable support separation is easily translated horizontally to accommodate capillaries of different length. Now the aluminium shield may be shifted in the profile, thus enabling it to be placed over the sample and aligned by a simple movement.

Heating is supplied by Kanthal A-1 resistive heaters (as described by Chupas *et al.*, 2008) mounted inside the aluminium shield, coiled around a ceramic tube and connected in parallel to the power supply *via* porcelain insulators. Power is provided by a direct current power supply (Delta Elektronika SM70-AR-24), which is regulated by a Eurotherm 2400 temperature controller on the basis of the sample temperature measured by the K-type thermocouple (0.25 or 0.5 mm). The thermocouple size was chosen in order to minimize heat transfer to the catalyst but at the same time assures enough temperature stability for the exothermic or endothermic reactions. For the cases studied here, capillaries from 0.5 mm up to 1 mm were paired with 0.25 mm-size thermocouples (Omega Engineering Inc., Model

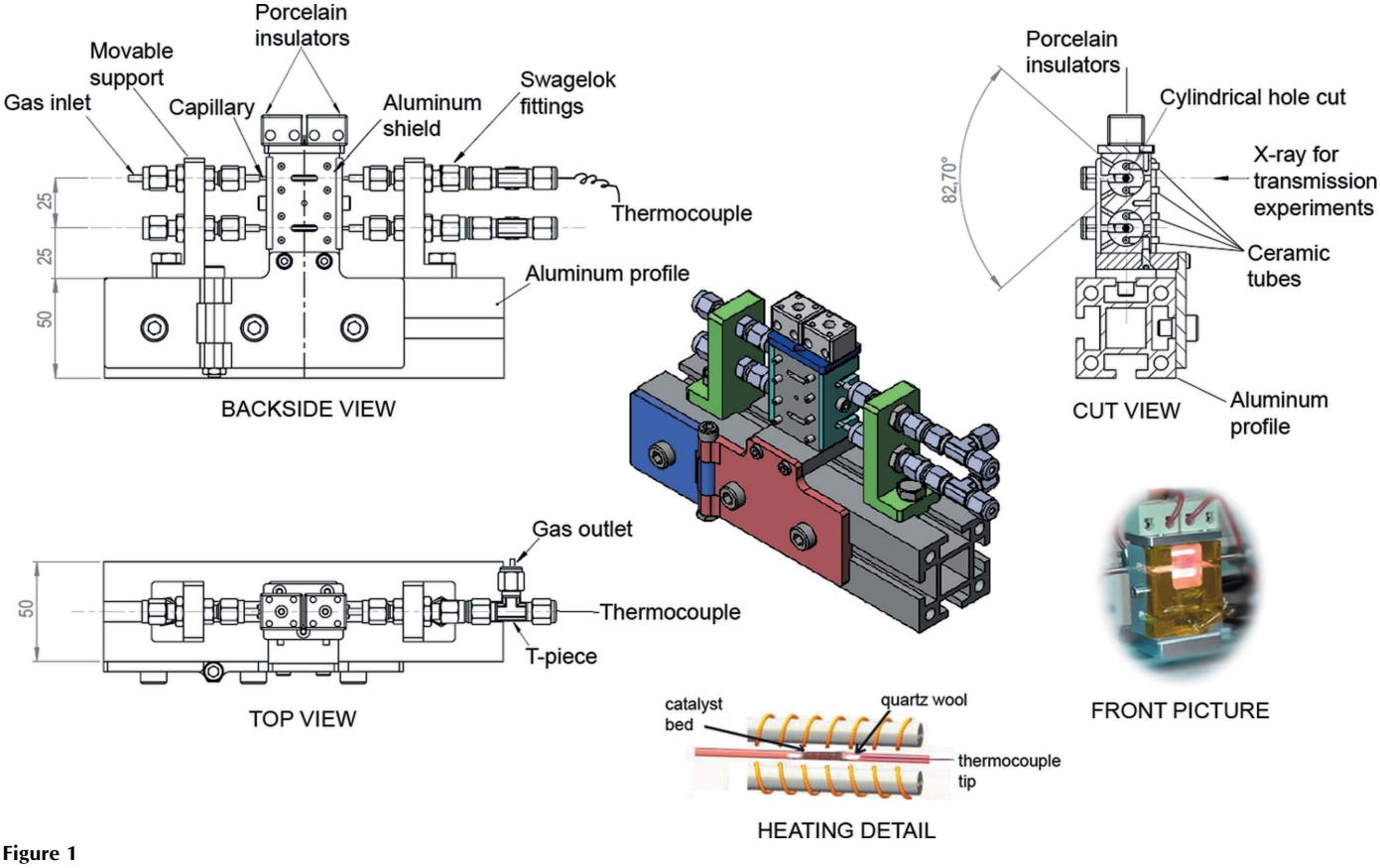

Figure 1
Microreactor technical design and components. At the center, the fully assembled flow cell/furnace is shown; several different views are sketched (top, backside and a cut view), to facilitate following the text. The heating detail illustrated shows the relative position of the catalyst bed and thermocouple tip in between the quartz wool. The 'front picture' is a photograph of the flow cell/furnace under working conditions at 1073 K; the Kapton tape is intended to avoid air currents that might suddenly change the temperature.

KMTIN-010U-6, 0.25 mm), and for capillaries from 1.1 mm up to 1.6 mm, a 0.5 mm-size thermocouple (Omega Engineering Inc., Model KMTIN-020U-6, 0.5 mm) was used.

As previously noted, aluminium has one of the best reflectivity coefficients for medium and far-infrared radiation (as much as 98%) (Wolfe & Zissis, 1993). The capillaries are held at the center of the cylindrical hole cut into the aluminium. This allows the IR radiation to be directly focused onto the capillary. The maximum working temperature reached exceeds the melting point of aluminium (933 K), but, as experimentally verified, the temperature on the shield does not exceed 500 K at the maximum working temperature. This occurs as an effect of the shield's reflective properties. The shield is further covered with a Kapton window to minimize convection cooling. As additional benefits, the electrical power and time response required to achieve a given target temperature are significantly reduced compared with the case where no aluminium shield is used.

As illustrated in Fig. 2, the thermal gradient along the 8 mm bed decreases when the temperature increases. This effect can be understood by keeping in mind that the dominant form of heat transfer at low temperatures is by natural convection, from higher- (the heaters) to lower-temperature regions (Kapton window), and at high temperatures the heat transfer is dominated by radiant heat transfer. Thus, the current use effectiveness of an IR reflective element increases with temperature, and therefore the temperature becomes more stable at higher temperatures where the heat transfer regime is close to being fully radiant (Rohsenow & Choi, 1961). With this design the axial thermal gradient along the bed was measured to be $\sim$0.13 K mm^{-1} at high temperatures under working conditions (space velocity of 15 000 h^{-1} in a 1 mm-diameter capillary with 0.025 mm wall thickness at temperatures ranging from 960 up to 1173 K). This value is slightly lower than that reported by Clausen *et al.* (1991) of $\sim$0.15 K mm^{-1} (3 K in 20 mm, using a gas blower as heating system), but unfortunately their work presents some uncertainties. They do not specify the wall thickness of the capillary used, if it is measured in flow or up to which temperature this reported gradient is valid. Thus it is difficult to perform an accurate comparative analysis between these two heating systems.

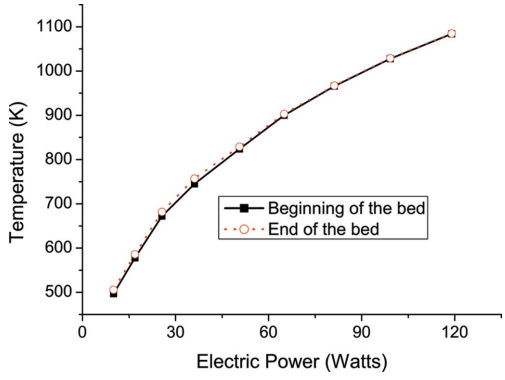

Figure 2
Electric power *versus* temperature for a 15 000 h^{-1} space velocity in a 1 mm-diameter capillary with a 0.025 mm wall thickness. This measurement was achieved using thermocouples inserted at both ends of the 8 mm bed.

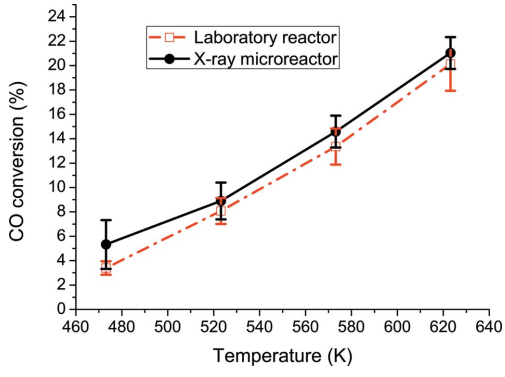

Figure 3
A comparison between the CO conversion for the water gas shift reaction of a standard laboratory reactor and that of the aluminium X-ray microreactor using a 10 wt% Cu in 12 wt% CeO_2/Al_2O_3 reforming catalyst as a function of temperature. Four measurements are taken at four different temperatures: 473, 523, 573 and 623 K; the errors are derived from the experimental results.

In order to compare the catalytic performance of the X-ray microreactor with a conventional laboratory reactor, the CO conversion of the water gas shift reaction obtained by a 12 wt% CeO_2 in 10 wt% Cu/Al_2O_3 reforming catalyst was measured four times at four different temperatures (see supplementary information for more experimental details[1]), as shown in Fig. 3. The differences in the conversion profiles for the X-ray microreactor and the laboratory reactor are less than 4%. Taking into account the associated error of the value estimation, the measurements are comparable. Differences can be ascribed not to temperature but to gas diffusion differences through the bed. Thus, the goal of achieving an *in situ* X-ray reactor design exhibiting close to the same conversion and behavior at equivalent residence times as a laboratory reactor has been met with this design for the typical catalytic reaction tested here.

As in their early work, Clausen *et al.* (1991) did not expect to be able to estimate the maximum pressure a capillary could support. On the basis of the work of Tekmen & Müller (2004), a theoretical estimation of the maximum pressure supported by the capillaries was calculated. The quartz capillaries used have a 1 mm diameter with a 0.025 mm wall thickness. The capillaries are calculated so as to resist 177 bar maximum internal pressure (this includes a factor of 3 as a safety factor). Consequently, the maximum (theoretical) working pressure, after the safety coefficient application, was $\sim$60 bar. It should be noted that in order to validate the microreactor the experimental test was restricted to 20 bar.

As discussed in the *Introduction*, a second capillary tube was incorporated (shown in Fig. 1 and in more detail in the supplementary information). This second tube has an independent entrance for gases, power supply and thermocouple, making it possible in principle to conduct other reactions simultaneously in the first capillary. This application is still under development. The commissioned uses of this second capillary are as a reference for dispersive EXAFS under a supported catalyst or diffraction reference, for non-simultaneous thermal treatments, and eventually to act as a substitute oven if there are problems with the first one. The aluminium housing containing both ovens has an inversion symmetry, making them completely exchangeable.

3. Applications

In the following section we show some brief examples of results obtained by using the microreactor on X-ray absorption near-edge structure (XANES) and XRD *in situ* experiments under *operando* conditions. Details of sample preparation and absorption as well as diffraction setup are given by Christoforidis, Figueroa *et al.* (2012)

[1] Supplementary material is available from the IUCr electronic archives (Reference: RG5025). Services for accessing this material are described at the back of the journal.

and Christoforidis, Iglesias-Juez *et al.* (2012). The studies were carried out on beamlines BM23 (Fe *K* edge, Si 111, $\Delta E/E = 2.0 \times 10^{-4}$) and ID15B (86.8 keV, $\lambda = 0.143$ Å, $\Delta E/E = 1.4 \times 10^{-3}$) at the ESRF. In this example the catalyst contains a few percent of iron (1.5% Fe-doped TiO_2). Thus, as we are interested in *in situ* XAFS experiments using the microreactor, the limitation on maximum capillary size (up to 1.6 mm) gives us an edge step lower than 0.1, requiring the experiment to be carried out in fluorescence mode. In this particular case the choice of an aluminium shield has practical advantages compared to stainless steel or other shields that may have their own intrinsic iron content and further completely avoids any potential interference from any background fluorescence coming from the shield or heaters, as experimentally shown. Another advantage of the chosen design is that it is possible to make the X-rays enter at 45° from the front side (Fig. 1, 'front picture'), allowing the simultaneous collection of transmission and fluorescence spectra.

Using the two X-ray techniques, we have investigated the effect of dopants (sulfur and iron) (*i.e.* local structure modifications) on the process of nucleation and growth of the anatase polymorph from amorphous powders. XAFS spectroscopy was applied in studying the effect of sulfur on the coordination environment and iron oxidation state in Fe-doped TiO_2 nanomaterials. As a natural result of *operando* experiments, we obtain a large number of spectra; for this reason XAFS data reduction was performed using *PrestoPronto* (Prestipino & Figueroa, 2010; Bordiga *et al.*, 2013), a specially developed code for handling large data sets such as the ones that can result from time- or space-resolved experiments coming from quick EXAFS and dispersive EXAFS beamlines. Fig. 4 presents representative Fe *K*-edge spectra in the XANES region under thermal treatment from room temperature up to 973 K at 5 K min^{-1} under dry synthetic air (20% O_2 in He, 10 ml min^{-1}). As explained by Christoforidis, Figueroa *et al.* (2012) these experimental results show that sulfur does not modify the local geometry and iron oxidation state in either amorphous or crystallized materials. Fig. 5 shows *in situ* diffraction data of a representative TiO_2 sample under a thermal treatment ramp. A mass spectrometer was fitted to the outlet of the flow microreactor, allowing the observation of the gaseous products evolved during the thermal treatment and offering advantages in quantifying the released gaseous products (H_2O, C, N and S based) and relating them to specific crystallization steps and/or the burning of organic moieties coming from the aqueous synthesis. These results are in close agreement with those obtained in the laboratory with a conventional reactor, giving additional support to the *operando* reactor behavior. The transition from amorphous to crystalline anatase structure can be observed. The broad diffuse features in the XRD pattern are characteristic of the amorphous structure developing gradually into a well crystallized anatase structure (JCPDS 21–1272). These *in situ* experiments further show that sulfur does not affect the onset of nucleation but rather the activation energy of the growth process of the anatase polymorph. This influences the primary particle size and shape of the nanomaterials (Christoforidis, Iglesias-Juez *et al.*, 2012). In addition, the microreactor was used to obtain *in situ* time-resolved X-ray total scattering data, as contained in the original design from Chupas *et al.* (2008), with the application of pair distribution function (PDF) analysis to obtain local structure information in the amorphous, intermediate and well crystallized states of TiO_2-based materials (Christoforidis *et al.*, 2013).

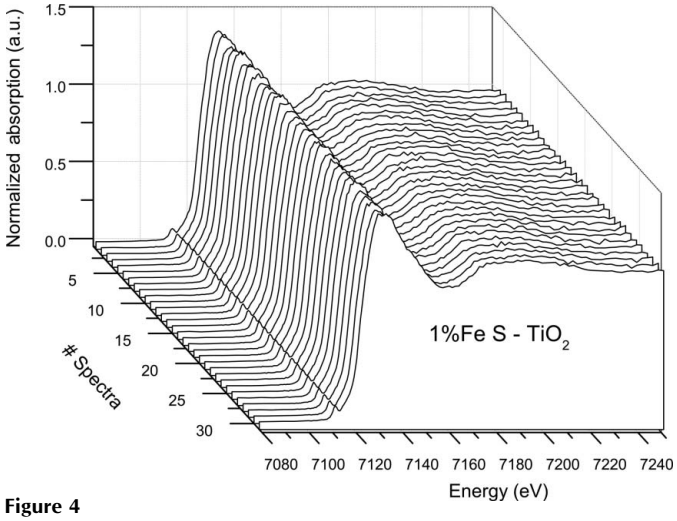

Figure 4
Fe *K*-edge XANES spectra obtained at BM23 in fluorescence mode, measured between 300 and 473 K.

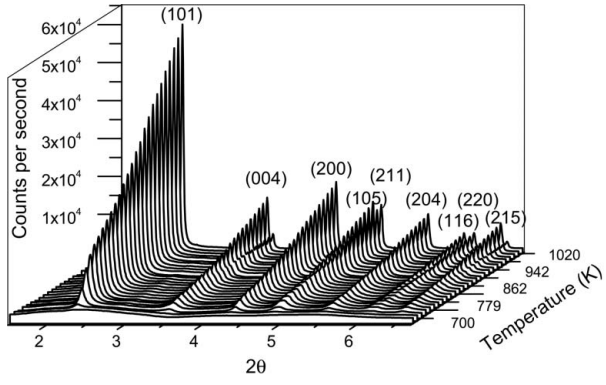

Figure 5
XRD diffractograms of a TiO_2 sample taken during an ID15B calcination ramp.

In summary, the use of a single setup for obtaining precise short- (XAFS; PDF-XRD) and long-range (PDF-XRD, XRD) information from the solid aided in obtaining a unified view of the structural parameters affecting nucleation and growth of a nanomaterial, thus providing key information to allow morphological control. The presence of anion and cation moieties was shown to alter a number of morphological properties that are considered as key to understanding the chemical (*e.g.* catalytic) properties of systems (Christoforidis, Figueroa *et al.*, 2012; Christoforidis, Iglesias-Juez *et al.*, 2012*b*; Christoforidis *et al.*, 2013).

4. Conclusions

The design and improvement of versatile plug flow microreactors aims to achieve, at a laboratory scale, the relevant industrial conditions of chemical processes that are still in development and are of ongoing significance. The development of the microreactor described here opens the possibility for new types of studies combining XAFS/XRD to probe the structural order of the short/long range and the kinetics of reaction at temperatures up to 1173 K. The correlation between the two experimental techniques is done in a straightforward manner using the same reactor. The innovative shield introduced in this new microreactor design effectively reduces the thermal gradients along a catalyst bed, yielding increased accuracy/precision in any given experimental situation. The overall efficiency of the reactor operation is also proportionally improved at high temperatures owing to the effect of the shield in focusing the radiation onto the capillary.

The authors acknowledge the European Synchrotron Radiation Facility for the provision of beam time on beamlines ID24, BM23 and

ID15. SJAF thanks Innokenty Kantor for some useful discussions on the model, and Hugo Vitoux and Florian Perrin for their contributions to the experiments. The authors gratefully acknowledge the help of Peter J. Chupas for providing the technical schematics of the original reactor system developed at Argonne National Laboratory, and Paula Caldas and José Maria Corrêa Bueno (UFSCar-Brazil) for the standard laboratory measurements included in Fig. 3. The research leading to these results has been funded by the Spanish CICYT (CTQ2010-14872/BQU) and the European Union's Seventh Framework Programme (FP7/2007–2013) under grant agreement No. 253445. KCC acknowledges Marie Curie Action – Intra-European Fellowship (FP7-PEOPLE-2009-IEF-253445) for a postdoctoral fellowship.

References

Bare, S. R., Kelly, S. D. & Mickelson, G. E. (2011). *Synchroton Rad. News*, **24**, 12–17.
Bare, S. R., Yang, N., Kelly, S. D., Mickelson, G. E. & Modica, F. S. (2007). *Catal. Today*, **126**, 18–26.
Beek, W. van, Safonova, O. V., Wiker, G. & Emerich, H. (2011). *Phase Transitions*, **84**, 726–732.
Bordiga, S., Groppo, E., Agostini, G., van Bokhoven, J. A. & Lamberti, C. (2013). *Chem. Rev.* **113**, 1736–1850.
Christoforidis, K. C., Figueroa, S. J. A. & Fernández-García, M. (2012). *Appl. Catal. B*, **117–118**, 310–316.
Christoforidis, K. C., Iglesias-Juez, A., Figueroa, S. J. A., Di Michiel, M., Newton, M. A. & Fernández-García, M. (2013). *Catal. Sci Technol.* **3**, 626–634.
Christoforidis, K. C., Iglesias-Juez, A., Figueroa, S. J. A., Newton, M. A., Di Michiel, M. & Fernández-García, M. (2012). *Phys. Chem. Chem. Phys.* **14**, 5628–5634.
Chupas, P. J., Chapman, K. W., Kurtz, C., Hanson, J. C., Lee, P. L. & Grey, C. P. (2008). *J. Appl. Cryst.* **41**, 822–824.
Clausen, B. S., Steffensen, G., Fabius, B., Villadsen, J., Feidenhans, R. & Topsøe, H. (1991). *J. Catal.* **132**, 524–535.
Grunwaldt, J., Caravati, M., Hannemann, S. & Baiker, A. (2004). *Phys. Chem. Chem. Phys.* **6**, 3037.
Jacques, S. D. M., Leynaud, O., Strusevich, D., Stukas, P., Barnes, P., Sankar, G., Sheehy, M., O'Brien, M. G., Iglesias-Juez, A. & Beale, A. M. (2009). *Catal. Today*, **145**, 204–212.
Li, S., Meitzner, G. D. & Iglesia, E. (2001). *J. Phys. Chem. B*, **105**, 5743–5750.
Meunier, F. C. (2010). *Chem. Soc. Rev.* **39**, 4602–4614.
Newton, M. A. (2007). *J. Synchrotron Rad.* **14**, 372–381.
Prestipino, C. & Figueroa, S. J. A. (2010). *PrestoPronto*, http://code.google.com/p/prestopronto/.
Rohsenow, W. M. & Choi, H. (1961). *Heat Mass and Momentum Transfer*. New York: Prentice Hall.
Tekmen, M. & Müller, J. D. (2004). *Rev. Sci. Instrum.* **75**, 5143–5148.
Wolfe, W. L. & Zissis, G. J. (1993). Editors. *The Infrared Handbook*. Ann Arbor: Environmental Research Institute of Michigan.